BULLETIN OF THE POLISH ACADEMY OF SCIENCES
TECHNICAL SCIENCES
Vol. 53, No. 4, 2005

Formation of bubbles and droplets in microfluidic systems

P. GARSTECKI[1,2*], A.M. GAÑÁN-CALVO[3], and G.M. WHITESIDES[2]

[1]Institute of Physical Chemistry, Polish Academy of Sciences, 44/52 Kasprzaka St., 01-224 Warsaw, Poland
[2]Department of Chemistry and Chemical Biology, Harvard University, 12 Oxford St., Cambridge, MA, USA
[3]Escuela Superior de Ingenieros, Universidad de Sevilla, 41092 Sevilla, Spain

Abstract. This mini-review reports the recent advances in the hydrodynamic techniques for formation of bubbles of gas in liquid in microfluidic systems. Systems comprising ducts that have widths of the order of 100 micrometers produce suspensions of bubbles with narrow size distributions. Certain of these systems have the ability to tune the volume fraction of the gaseous phase – over the whole range from zero to one. The rate of flow of the liquids through the devices determines the mechanism of formation of the bubbles – from break-up controlled by the rate of flow of the liquid (at low capillary numbers, and in the presence of strong confinement by the walls of the microchannels), to dynamics dominated by inertial effects (at high Weber numbers). The region of transition between these two regimes exhibits nonlinear behaviours, with period doubling cascades and irregular bubbling as prominent examples. Microfluidic systems provide new and uniquely controlled methods for generation of bubbles, and offer potential applications in micro-flow chemical processing, synthesis of materials, and fluidic optics.

Key words: formation of bubbles and droplets, microfluidic systems, hydrodynamic techniques.

1. Introduction

Interfacial dynamics in microfluidic systems – systems of channels of at least one characteristic dimension on the order of 10 to 100 μm – has been the subject of intense interest in the last years, starting with the work by Thorsen et al. [1] on formation of droplets in microfluidic T-junction geometries, and the work of one of the authors [2,3] on formation of bubbles in axi-symmetric capillary flow-focusing devices. Microfluidic systems offer convenient methods for highly controlled formation of gas-liquid and liquid-liquid emulsions. Break-up in microfluidic systems typically occurs in co-flow – that is when both phases flow along the gradients of pressure – and in confinement by the walls of the devices. Recent research, together with decades of study [4] of interfacial dynamics, help to understand the non-linear, dynamic phenomena of emulsification. Here we briefly review recent results in micro-emulsification, and in the use of flows of droplets and bubbles in microfluidic systems. We discuss both the background in this area, and our recent work on generation of gaseous bubbles in micro-systems; our discussion includes planar devices operating at low values of Reynolds and capillary numbers, and axi-symmetric systems that form bubbles at high values of Reynolds and Weber numbers. Both types of systems are capable of producing monodisperse bubbles, with precisely tuned diameters from few to hundreds of micrometers. Surprisingly, in both cases, the interfacial tension does not enter the scaling relations for the volumes of the bubbles. At low capillary numbers, the dynamics of break-up is controlled by the balance of pressures in the liquid and gas. At high Weber numbers, interfacial forces are negligible in comparison with inertial effects. Interestingly, the transition between the two regimes – when the interfacial tension does play a role comparable to the inertial stresses – exhibits phenomena that are diagnostic of non-linear systems: bifurcations, period doubling cascades, and chaotic bubbling. Although difficult to control, these non-linear processes open a potential route to emulsions characterized by multimodal distribution of size.

We begin with a short – and certainly focused and incomplete – survey of microfluidic systems, with particular emphasis on generation and use of multiphase flows. We follow with a description of the systems that we have studied, and of their dynamics. Conclusions include a summary of the results, and speculation about possible future directions for research, and potential applications.

1.1. Microfluidics. The exquisite control that microfluidic systems afford over flows of liquids of normal viscosities stems from the fact that flow at this scale, and at typically used volumetric rates of flow, is dominated by viscous effects. The values of the Reynolds number ($Re = \rho u l/\mu$, with ρ and μ being the density and dynamic viscosity of the fluid respectively, u the speed of flow, and l the characteristic dimension of the system) are often small: $Re \ll 1$, or – at most – moderate $Re < 100$. Flow is laminar, and the streamlines of the fluids can be precisely controlled by an appropriate design of the geometry of the channels. The intense interest in microfluidic systems in the last decade has been sparked by the introduction of inexpensive and simple methods for fabrication of the devices. Soft lithography [6] and the use of elastomeric molds, such as poly(dimethylosiloxane) (PDMS) [7], have been especially useful, since they allow ideas to be converted to devices with turn-around time much less than those characteristic of conventional silica micromachining.

*e-mail: garst@ichf.edu.pl

Flows at sub-millimeter length scales can be 'engineered': it is possible to design and generate desired distributions of chemical concentration or temperature in the channels; microfluidics also uses small quantities of fluids. These features have already found – and continue to lead to – a host of applications [8], chiefly in creating tools for research in biology [9,10], and for chemical processing – e.g. high-throughput screening [11], immunoassay [12,13], or development of organic reactions [14].

1.2. Micro-emulsification. Controlled formation of droplets has a variety of uses – from ink-jet printing to industrial processing [15] – and recent progress in design and use of microfluidic systems [16] has generated novel microfluidic techniques for highly controlled emulsification. The first truly microfluidic, on-chip, droplet generator was reported by Thorsen et al. [1] who used a T-junction geometry to generate aqueous droplets in an organic continuous phase. In this geometry the immiscible (to-be-dispersed) fluid is fed into a main channel that carries the continuous fluid. This continuous fluid wets the walls of the channels preferentially, and as the immiscible, non-wetting, phase enters the main duct, it breaks into droplets. Thorsen et al. [1] explained the observed scaling of the size of the droplets by a competition between the shear stresses exerted on the tip of the discontinuous phase by the host, or carrier fluid and the interfacial tension that opposed the elongation of this tip in the downstream direction. Typical values of the capillary number ($Ca = \mu u/\gamma$, where γ is the interfacial tension)-number that describes the ratio of viscous to interfacial stresses-for these experiments were on the order of $Ca \sim O(10^{-2})$ and larger. At lower values of the capillary numbers, the main contribution to the break-up dynamics arises from the build-up of pressure in the continuous phase upstream of the tip of the discontinuous phase, as, at low values of Ca, this tip effectively blocks the main channel [17] and confines the continuous fluid to thin, wetting films. This mechanism of break-up-driven by normal, rather than tangential stresses exerted on the emerging droplet by the continuous fluid is specific to confined (microfluidic) systems. In spite of the fact that interfacial stresses dominate both the shear stresses, and gravitational effects (capillary lengths are typically much larger than the widths of the channels) in this regime the size of the droplets generated in the T-junctions is independent of Ca and follows a simple relation involving only the ratio of the volumetric rates of flow of the two immiscible fluids [17]. The T-junction [18], and variants [19] of this geometry, are used in a host of applications, including chemical analysis [20,21], screening of conditions for protein crystallization [22, 23], formation of solid, non-spherical particles [24], and formation of double emulsions [25].

The second class of systems that is used to generate emulsions in microsystems encompasses geometries in which the continuous fluid is forced through a narrow constriction in the main channel, and the discontinuous fluid – dispensed from a nozzle located closely upstream of the constriction – is focused into this orifice by the converging streamlines of the carrier fluid. An axi-symmetric flow-focusing system has been demonstrated [2,3] to generate highly monodisperse bubbles in liquids. A similar, axi-symmetric geometry provides convenient methods of obtaining double-emulsions [26] and chemical processing of droplets to obtain microcapsules characterized by narrow size distributions [27]. Implementation of the concept of flow-focusing onto a planar microfluidic device [28] followed with a number of studies of this (planar) geometry, including studies on formation of droplets [29,30], and bubbles [31–33].

Other methods are available for highly controlled generation of emulsions at microscale: – interesting examples include geometrically mediated break-up of droplets in T-shaped branching channels [34], break-up in micro-terrace geometries [35], emulsification on membranes [36,37], or parallel microdispensing [38].

1.3. Synthesis of anisotropic particles in microfluidic channels. The ability to form monodisperse droplets in microfluidic systems and the feature offered exclusively by the use of microchannels – that of strong geometrical confinement of the droplets – provides new methods for generation of monodisperse particles with remarkable control of their shapes. Often the droplets generated in the microchannels have volumes that exceed the volume of the largest sphere that can be inscribed in the cross-section of the channel, and the droplets assume either discoid shapes (when the height of the channel is much smaller than its width), or elongated, rod-like ones (when the interface of the droplet rests on both the top/bottom and the side walls of the channel). When the droplets – or streams of fluid – are solidified in-situ, in the channel, they become anisotropic particles of characteristic dimensions from tens to hundreds of micrometers [24,39–42]. These two-step processes (first make a droplet, than polymerize it) rely on hydrodynamic rather than physico-chemical mechanisms and are largely independent of the chemical composition of fluid that forms droplets. This freedom to alter the composition of the droplets (and thus particles) without affecting the process of formation of the droplets (and thus their size and shape) allows for combination of the basic technique described above with a range of physico-chemical processes that further enhance the structure and functionality of the synthesized particles – for example: i) the use of a blend of polymers that subsequently phase-segregated allowed formation of monodisperse porous particles [43]; and ii) the use of multiple immiscible phases allowed formation of particles with internal structure [44]; or iii) the use of gels provided a way for entrapment of living cells [45]. An interesting, additional, capability offered by microfluidic systems is that of arraying droplets into large, periodic arrays [46], with a potential use in optics [47].

1.4. Droplet-beakers. Much interest in formation of droplets and bubbles in microfluidic systems is motivated by the prospect of conducting chemical reactions and analyzes inside droplets. In these experiments, the droplets serve as miniature 'beakers' [48, 49]. Microfluidics makes it easy to prepare – with control, and in large quantities – droplets having a range of chemical composition [50], to coalesce droplets

composed of different solutions [51], to mix the content of the droplets effectively [52], and to observe, and measure the kinetics of reactions proceeding inside drops [20]. Demonstrations of components of an on-chip-laboratory operating on droplets are already available. These components include systems for screening of reaction conditions [50], and conditions to use for protein-crystallization [22,23], for organic microsynthesis [14], and procedures for encapsulation and lysis of cells [53]. The outstanding goal of this subfield of microfluidics is the ability to design a system in which every droplet can be individually prepared, processed and analyzed [54]. Reaching this goal requires control over the times at which droplets are produced, and over the paths that the droplets take through the networks of microchannels that constitute the miniature 'laboratory'. Various efforts to achieve this goal include, for example, the use of electro- [55–57] or thermo- [58] capillary effects to control formation and flow of the droplets.

1.5. Segmented flow. Flow of an emulsion through a capillary, with the droplets filling the cross-section of the capillary and thus dividing the continuous fluid into 'segments', has a history of use in chemical processing [59,60]. Recent interest in microfluidics has revived interest in segmented flow [61] and used it to compartmentalize [62,63] and mix [64–67] the continuous fluid. The convective rolls [68] that recirculate the continuous fluid in between the immiscible slugs homogenize the distribution of the residence time of the continuous fluid in the channel; this effect has been exploited to develop a continuous-flow preparation of silica colloids [69].

1.6. Controlled formation of bubbles in microfluidic systems. In the following sections we review our recent results on formation of bubbles in microfluidic systems having typical dimensions of the channels or capillaries on the order of tens and hundreds of micrometers. We were interested in both the low Reynolds and low capillary numbers flows in planar geometries, and in the high Reynolds and high Weber numbers flows in axi-symmetric capillary flow-focusing systems. We describe each below, including the details of the experimental procedures and the major findings on the dependence of the size of the bubbles on the material and flow parameters of the fluids, and on the geometry of the devices. The two classes of systems exhibit different mechanisms of emulsification, as different forces dominate the dynamics of break-up. The unifying feature – although it is observed for very different reasons – is that both systems produce bubbles characterized by narrow size distributions, and that the interfacial stresses do not influence the size of the bubbles. Surprisingly, when the interfacial stresses are comparable to other forces, the bubbles are no longer monodisperse and we observe dynamics that is typical for transitions to chaos in non-linear systems.

2. Formation of bubbles at low values of the capillary number

2.1. The microfluidic flow-focusing device, materials and methods. Figure 1 shows a micrograph and a schematic illustration of the typical system that we used [31,32,70] for formation of bubbles in planar microfluidic devices. The channels, fabricated using soft-lithography [6,7] have uniform height h. This height (typically $h \sim 30$ μm) is small in comparison with lateral dimensions of the device: the widths of the channels range from tens to hundreds of micrometers and their lengths are from hundreds of micrometers to few centimetres. We assembled the devices by sealing oxidized PDMS replicas of the planar network of channels onto oxidized glass cover slides [7]. If the continuous phase does not wet the walls of the channels, flow patterns are disordered [71]. Stable formation of bubbles in aqueous solutions requires that the walls of the device are hydrophilic, and are wetted by the continuous (aqueous) phase (Fig. 1c). In order to preserve the hydrophilic character of oxidized surfaces, we filled the channels with water immediately after sealing. The contact angle of aqueous solutions used in our study on freshly oxidized PDMS was less than 30°. We supplied the two immiscible fluids (nitrogen gas and aqueous solutions of glycerol and surfactant Tween 20) to the device via PET tubing. We drew the gas from a pressurized tank via a pressure-reduction valve; the liquids were pumped using a syringe pump (Harvard Apparatus PhD2000). In order to test the influence of viscosity of the continuous fluid on the process of formation of bubbles, we used a aqueous solutions of glycerol [31,32,70]. All of the liquids contained 2% (w/w). Tween-20 surfactant to stabilize the bubbles against coalescence; we used liquids without surfactant only in experiments in which we tested the influence of the value of interfacial tension on the process of break-up. The system usually required a short time (on the order of tens of seconds) to come to a steady-state inflow of the two fluids after changing any of the flow parameters. PDMS is a transparent elastomer; this property makes it straightforward to monitor the behaviour of the systems with the use of optical microscopy. We used a Nikon camera to capture still images, Phantom high-speed cameras to capture movies, and custom made tools for image analysis to measure the areas of the interface between the bubbles and the top wall of the channel.

2.2. Formation of bubbles. Qualitatively, the operation of the flow-focusing device [28,31] illustrated in Fig. 1 can be described as follows. The two immiscible phases flow down the inlet channels (one central channel for gas, and the two outer channels for liquid) and meet at the junction of these channels upstream of the orifice. The pressure drop along the axis of the system forces the fluids through this orifice; the tip of the stream of gas enters the orifice and inflates a gas cavity downstream of the orifice. This cavity (a growing bubble) displaces and pushes away the liquid in the outlet channel. Subsequently the neck connecting the inlet for the gas with the growing bubble breaks, and the bubble is released in the outlet channel. We observed that over a wide range of pressures (p) applied to the stream of gas, and of rates of flow (Q) of the liquid, the system establishes a periodic state, in which, in each period, the tip enters the orifice, inflates a bubble, breaks, and retracts upstream of the orifice. The bubbles are uniform in size. The measured standard deviation of the diameters of the interfaces between

the bubbles and the top wall of the outlet channel was typically smaller than five percent of the mean value of this diameter. The size of the bubbles could be easily tailored: for a constant pressure applied to the stream of gas, an increase in the rate of flow of the liquid resulted in a decrease of the volume of the bubbles; for a fixed rate of flow, an increase of pressure resulted in an increase of the size of the bubbles.

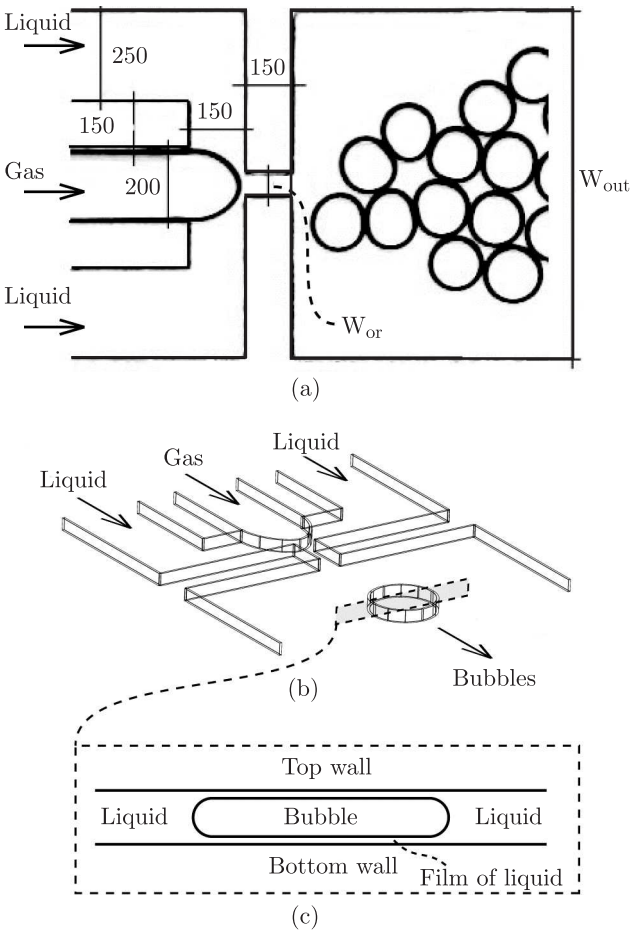

Fig. 1. A micrograph of a typical flow focusing device that we used in our studies on formation of bubbles at low values of capillary numbers (top view). The device is planar; the channels have uniform height (typically h = 20–40 μm). The dimensions in the plane of the device are given in the figure (in micrometers). In the device shown in the micrograph, the width of the orifice is $w_{\rm or}$ = 60 μm, and the width of the outlet channel is $w_{\rm out}$ = 1 mm (a); a schematic illustration showing the aspect ratio of the height of the device to the widths of the various channels; typically the height is much smaller than the lateral dimensions. The liquid is delivered via the two outer inlet-channels and the gaseous phase through the channel running along the centreline of the device. The stream of gas is focused by the streams of liquid into the orifice and breaks there to release bubbles into the outlet channel (b); In order to achieve a stable operation of the system, the walls of the device have to be preferentially wetted by the continuous (in our experiments aqueous) phase. As a result the gas does not wet these walls and the gas-liquid interface is always separated from the walls by thin, wetting films of the carrier fluid (c)

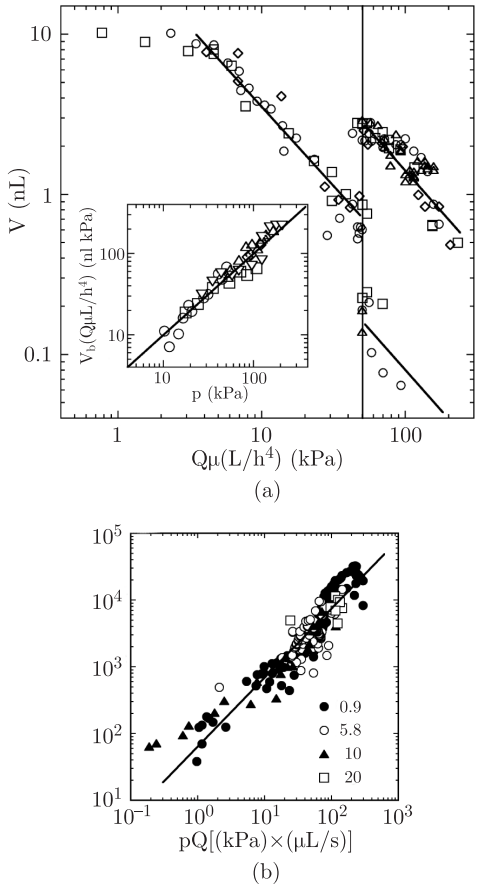

Fig. 2. Volume of the bubbles produced in a planar microfluidic device plotted against the product of the rate of flow Q and viscosity μ of the liquid, and scaled to the units of pressure by multiplying by L/h^4, where L is the length of the outlet channel and h is its height. All experiments shown in this figure were performed with $p = 27.6$ kPa and with following geometrical parameters: $w_{\rm or} = 30$ μm, $w_{\rm out} = 750$ μm, and $L = 30$ mm. Symbols correspond to different viscosities and interfacial tensions (○) $\mu = 0.92$ mPa, $\gamma = 37.0$ mN/m; (△) $\mu = 0.92$ mPa, $\gamma = 72$ mN/m (□) $\mu = 6.1$ mPa, $\gamma = 31.6$ mN/m and (◇) $\mu = 10.84$ mPa, $\gamma = 33.1$ mN/m. The solid lines give the slope of a relation $(q\mu)^{-1}$. At the rate of flow marked by the vertical line, the formation of bubbles bifurcates and produces bubbles of two different sizes. The inset shows scaling of the bubble size with pressure. Five series of data are shown for ($\mu = 0.92$ mPas, $\gamma = 37$ mN/m) and five different flow rates: (○) 0.278 (□) 0.556, (◇) 1.39, (△) 2.78, and (▽) 5.66 μL/s. We multiplied V_b by $(q\mu L/h^4)$ to leave only the dependence on pressure. The solid line gives the slope of a linear relation between V_b and p (a). The frequency of bubbling, plotted against the product (pQ). Different symbols correspond to different viscosities μ of the liquid (values in [mPa s] given in the legend). The solid line shows the fit $f = \alpha(Qp)^\beta$, with $\alpha = 53.3$ and $\beta = 1.04$ (regression coefficient R = 0.94) (b). Inset a is adapted (after Ref. 31), and inset b (after Ref. 70)

We explored experimentally the dependence of the size of the bubbles on the accessible parameters of the system: the pressure (p) applied to the gas stream, the rate of flow (Q) of the liquid, the dynamic viscosity (μ) of the liquid and the interfacial tension (γ) between the two phases. We found that the volume V of the bubbles scales as (Fig. 2a):

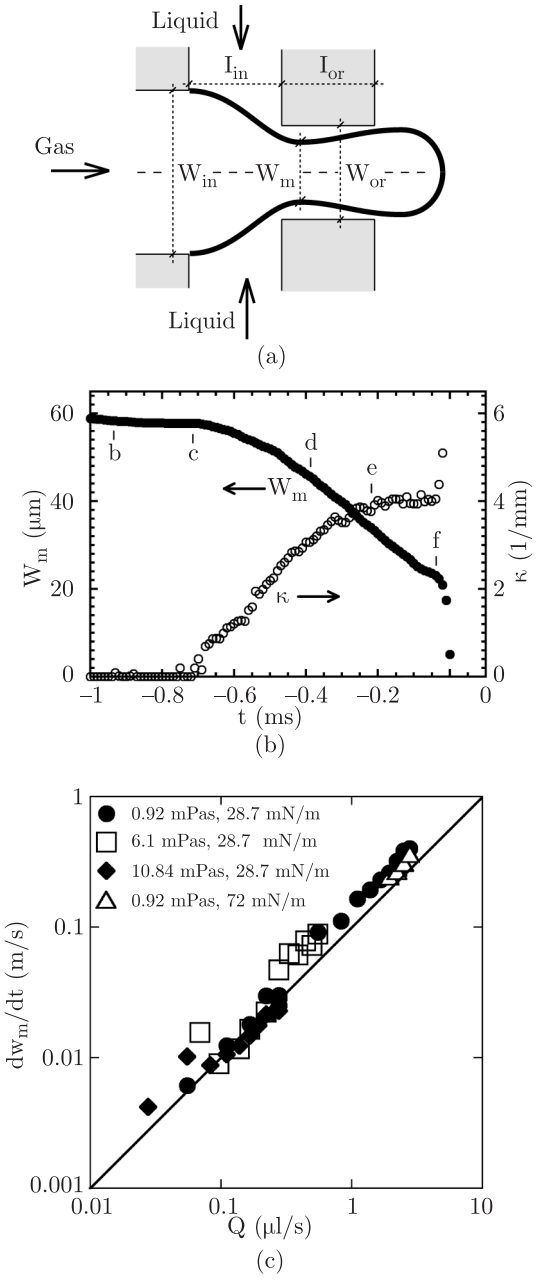

Fig. 3. Schematics of the orifice region and the gas-liquid interface. The shaded areas correspond to PDMS walls and the long-dashed line marks the centreline and axis of mirror symmetry of the channel. The scheme defines the dimensions of the orifice region: the width of the gas-inlet channel ($w_{\rm in} = 200$ μm), the distance between this inlet and the orifice ($l_{\rm in} = 150$ μm), the width ($w_{\rm or} = 60$ μm) and length ($l_{\rm or}$) of the orifice. Our experiments varied h (28, 36 and 64 μm) and $l_{\rm or}$ (50, 100, 150, 250 μm). For the analysis of breakup, we trace the evolution of the minimum width w_m of the gaseous thread and its axial curvature κ at this minimum (a). Evolution of the minimal width w_m, and the axial curvature κ of the gas-liquid interface in a typical break-up event ($l_{\rm or} = 100$ μm, $h = 36$ μm, $q = 0.56$ μL/s, $p = 34.5$ kPa, $\mu = 0.9$ mPa s, and $\gamma = 28.7$ mN/m) (b). A log-log plot of the speed of collapse (dw_m/dt) plotted against the flow rate of the continuous fluid q ($l_{\rm or} = 150$ μm, $h = 28$ μm). The gas pressure was set to $p = 69$ kPa (10 psig). The values of viscosity and surface tension for each series are given in the figure (c). Graphs adapted (after Ref. 32)

$$V/V_{\rm or} \propto \left(p/Q\mu(h^3 w/L)\right) \tag{1}$$

where $V_{\rm or}$ is the volume of the orifice, h, w and L are the height, width and length of the outlet channel respectively. We also found an approximate, empirical relation for the frequency f of bubbling as a function of p and Q (Fig. 2b):

$$f \propto pQ/C \tag{2}$$

where C is a constant expressed in units of energy. Following Eq. 1, for a given viscosity of the liquid, the volume of the bubble depends only on the ratio of p to Q, while the frequency depends on the product of these two parameters. This dependence is equivalent to a transformation of variables (3)

$$(p, Q) \rightarrow (V, f) \tag{3}$$

and allows a simultaneous and independent control of the volume of the bubbles and the frequency at which they are generated. By keeping the ratio of p/Q constant, we can control the volume fraction of the dispersed phase, defined as $\phi = fV/(fV + Q)$, for any (fixed) size of the bubble. This feature makes the microfluidic flow-focusing technique particularly attractive for preparation of suspensions of bubbles with tailored properties, especially as ϕ can be tuned over the whole range, from almost zero to almost one [31].

2.3. Dynamics of break-up. Equations 1 and 2 are interesting because the value of interfacial tension (γ) does not enter them. This absence is intriguing because the experiments for which Eqs 1 and 2 hold are conducted at low values of the capillary number $Ca = u\mu/\gamma$, (here u is the characteristic speed of the liquid, calculated as $u = Q/A$, with A denoting the cross-section of the orifice): in our experiments [31,32] typical values of Ca range from 10^{-3} to 10^{-1}, indicating that interfacial forces should dominate the shear stresses. The lack of dependence of the size of the bubbles on the value of the interfacial tension made it impossible to identify clearly the mechanism of break-up in microfluidic flow-focusing devices. In order to understand the dynamics of break-up we conducted a series of experiments with a range of rates of flow and viscosities of the liquid, pressures applied to the gas-stream and values of interfacial tension [32], and we monitored the evolution of the shape of the gas-liquid interface during the process of break-up. Figure 3a illustrates schematically the profile of the tip of the stream of gas, and Figure 3b shows a generic shape of the curves, and illustrate the evolution of the minimum width $(w_{\rm m})$ of the gaseous thread and of the axial curvature (κ) of the interface at the point of minimum width. At first, after the tip of the stream of gas enters the orifice, fills it almost completely and the interface rests on the walls of the orifice, separated from them only by thin wetting films of the continuous fluid. In this stage the minimum width of the neck stays constant and is similar to the width of the orifice: $w_{\rm m} = w_{\rm or}$. Subsequently the neck connecting the inlet channel for gas with the bubble growing in the outlet channel starts to thin, and $(w_{\rm m})$ decreases approximately linearly in time. Finally, the neck breaks rapidly, the tip of the stream of gas retracts upstream, and the whole process repeats. The

curvature $\kappa \approx 0$ in the first stage, it grows monotonically in the second stage (during the 'linear' collapse of the neck) and diverges quickly during the final rapid break-up. Since these general features of the evolution of the minimum width with time are generic for the system over a wide range of rates of flow, viscosities of the liquid, pressures applied to the stream of gas, and values of interfacial tension, we used the rate of the approximately linear decrease of (w_{m}) in the second stage to quantify the 'speed of collapse' u_{collapse} as a function of all the parameters that we changed. We found, that this rate does not depend on either p, μ, or γ, and it depends only (and linearly, Fig. 3c) on the rate of flow of the continuous fluid Q:

$$u_{\mathrm{collapse}} \approx dw_{\mathrm{m}}/dt \propto Q \tag{4}$$

The speed of collapse u_{collapse} that we recorded in our experiments is also small in comparison with order-of-magnitude estimates of the speed of relaxation of curvature of an interface driven by interfacial tension. Estimates of the expected 'natural' speed of collapse driven by interfacial tension yield $u_{\mathrm{VISC}} \approx \gamma\mu$, or $u = u_{\mathrm{INERT}\approx(\gamma/\rho \mathrm{L})^{1/2}}$ depending on whether viscous or inertial terms dominate the dynamics of the system (L denotes a typical radial dimension). The Ohnesorge number Oh = $\mu/(\rho\gamma L)^{1/2}$, where ρ is the density of the liquid ($\rho = 10^3$ kg/m^3) calculated for our experiments, yields Oh = $\mu/(\rho\gamma L)^{1/2} \approx 0.06$ (for $L = 10$ μm, and water-surfactant mixture as the liquid: $\mu \approx 1$ mPas, $\gamma \approx 30$ mN/m), and, consequently, $u_{\mathrm{INERT}} \approx 2$ m/s. For the most viscous water-glycerol-surfactant mixture that we used in our experiments ($\mu \approx 10$ mPas), Oh ≈ 0.6, and $u_{\mathrm{VISC}} \approx 2$ to 3 m/s. These estimates are one to three orders of magnitude larger than the speed of collapse that we measured in our experiments (Fig. 3c).

2.4. Mechanism of break-up. We have shown [32] that the above observations are well explained by the noticing that neck connecting the inlet channel for gas with the bubble growing in the outlet channel is stable with respect to interfacial forces. We have modelled the interface spanning from the end of the inlet channel for gas to the exit of the orifice using the Surface Evolver package [72] and we found a family of stable shapes of the gas-liquid interface parameterized by the volume of gas enclosed by this interface. We have also compared experimentally measured minimum widths of the neck, plotted as a function of the volume of liquid pumped into the orifice (tQ), with the minimum width obtained from the simulations and expressed as function of (minus) the volume enclosed by the interface. We found that the experimental measurements obtained for a wide range of flow parameters overlap with the numerical prediction [32].

The process of break-up can be explained as follows: as the tip of the stream of gas enters the orifice, it confines the liquid to thin films between the gas-liquid interface and the walls of the orifice. Flow in thin films is associated with high pressure gradients that scale (within the lubrication approximation) as $\Delta p \propto d^{-3}$ [73]. As the liquid is pumped into the orifice region at a constant rate, the confinement of the liquid to thin films leads to an increase of pressure in the liquid upstream of the orifice. As a result the liquid displaces the gas at a rate proportional to its volumetric rate of flow. The time t_{collapse} that it takes to collapse the neck of the stream of gas that has entered the orifice is on the order of $t_{\mathrm{collapse}} \approx O(Q/V_{\mathrm{or}})$, where V_{or} is the volume of the orifice.

An important feature of this mechanism of break-up is that it is slow: u_{collapse} is much smaller than the typical rates of relaxation of the curvature of the interface. Thus, as the inflowing liquid 'squeezes' the neck connecting the inlet for gas with the growing bubbles, the interface rapidly equilibrates to the new boundary conditions (determined by the volume of the liquid in the orifice) and, as a result, the break-up proceeds through a series of equilibrium states. All fluctuations in the rate of flow, pressure, temperature and other parameters are equilibrated at time-scales that are much shorter than the rate of collapse, and that average out on the scale of t_{collapse}. This separation of time scales for the break-up and equilibration of the curvature of the interface and pressure fields in the liquid lead to the very reproducible break-up – formation of each bubble is virtually the same and so are the sizes of the bubbles produced this way.

The rate-of-flow-controlled mechanism of break-up is specific to microfluidic systems and cannot be observed in break-up of immiscible threads in an unbounded fluid. One of the prerequisites for this dynamics is that the interfacial dynamics-the evolution of the shape of the interface-is strongly affected by the presence of the walls of the device. This condition can be expressed in low values of the capillary number, and in large ratios of the capillary lengths in comparison with the typical length-scales of the device (e.g. width of the orifice). The rate-of-flow-controlled break-up explains the scaling of the volume of the bubbles depicted in Eq. 1. The volume of the bubble is proportional to the time during which the stream of gas feeds the emerging bubble, multiplied by the rate of inflow of gas into it. The time during which the neck stays open is proportional to the collapse-time t_{collapse}, which in turn is inversely proportional to the rate of flow of the liquid: $t_{\mathrm{collapse}} \propto Q^{-1}$. Because, during the collapse of the gaseous thread, the flow of liquid into the outlet channel is restricted, the rate of inflow of gas into the bubble Q_{inflow} is equal to the total rate of flow in the outlet channel: that is, an emerging bubble pushes the fluid that is present in the outlet channel downstream. The flow in the outlet channel is subject to dissipation, which – to a first approximation, and taking into account the low values of the Reynolds number for this flow – is proportional to the viscosity of the liquid. Thus the rate of flow in the outlet channel is proportional to the pressure applied to the emerging bubble $(\sim p)$ and inversely proportional to the vscosity of the continuous fluid μ. Finally, Eq. 5 describes the volume of the bubble in terms of Q, p, and μ:

$$V \propto t_{\mathrm{collapse}} Q_{\mathrm{inflow}} \propto (1/Q)(p/\mu) \tag{5}$$

recovering the experimentally observed scaling of V (1). Interestingly, by approximating the rate of flow of gas Q_{gas} by the rate of inflow of gas into the bubble $Q_{\mathrm{gas}} \sim Q_{\mathrm{inflow}}$, Eq. 5 can also be expressed in terms of the ratio of the rates of flow of the two immiscible fluids: $V \propto Q_{\mathrm{gas}}/Q$.

2.5. 'Selective withdrawal' of bubbles in planar geometries. Another method similar to flow-focusing, and one that could be considered a two-dimensional version of the selective withdrawal [74,75] technique for generation of microbubbles has been reported recently [33]. The system is planar and consists of a large, rectangular chamber of a small height h (a Hele-Shaw like cell) with a single outlet. The liquid is delivered to the chamber from the two sides of this orifice, and gas is pumped into the chamber from an inlet located upstream of the orifice (Fig. 4). In the experiments reported in [33], the device operated at moderate values of Reynolds numbers ($Re \sim O(100)$) and at capillary numbers greater than 1 ($Ca \sim O(10)$). The device can be tuned by adjusting the pressures applied to the streams of liquid and gas to produce bubbles with diameters ranging from few micrometers to hundreds of micrometers, and – importantly – at high volume fractions of the gaseous phase. In this system – operating at moderate values of Re – the volume of the bubble presented two distinct forms of dependencies on the ratio of $(Q_{\rm gas}/Q_{\rm liquid})$. For $(Q_{\rm gas}/Q_{\rm liquid} > 1)$ the volume of the bubbles scaled as (6):

$$d/D \propto Q_{\rm gas}/Q_{\rm liquid} \tag{6}$$

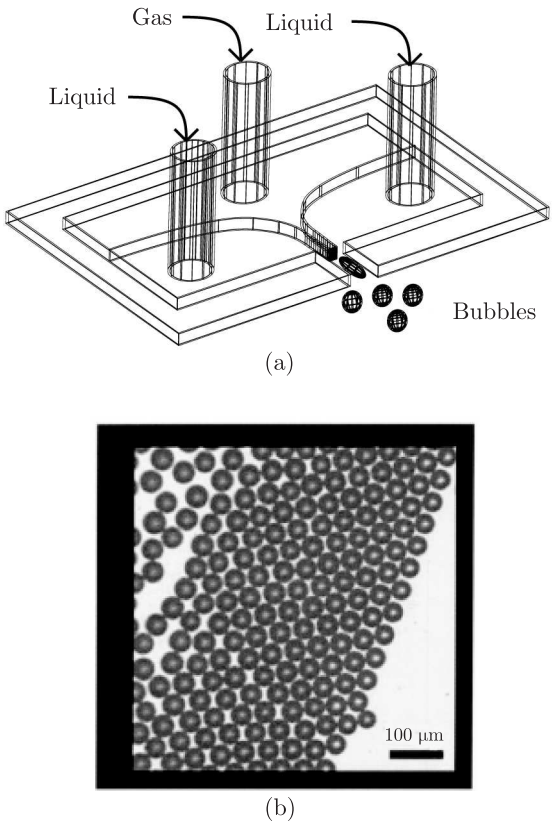

Fig. 4. A schematic illustration of the planar device used to produce bubbles at high volume fractions (after Ref. 33). Both phases are delivered into a chamber that has a single outlet in the plane of the device – i.e. an orifice. The stream of gas – focused by the two streams of liquid – breaks in the orifice to produce bubbles (a). Inset b) shows a representative micrograph of the suspension of bubbles produced in this device. Inset is b adapted (after Ref. 33)

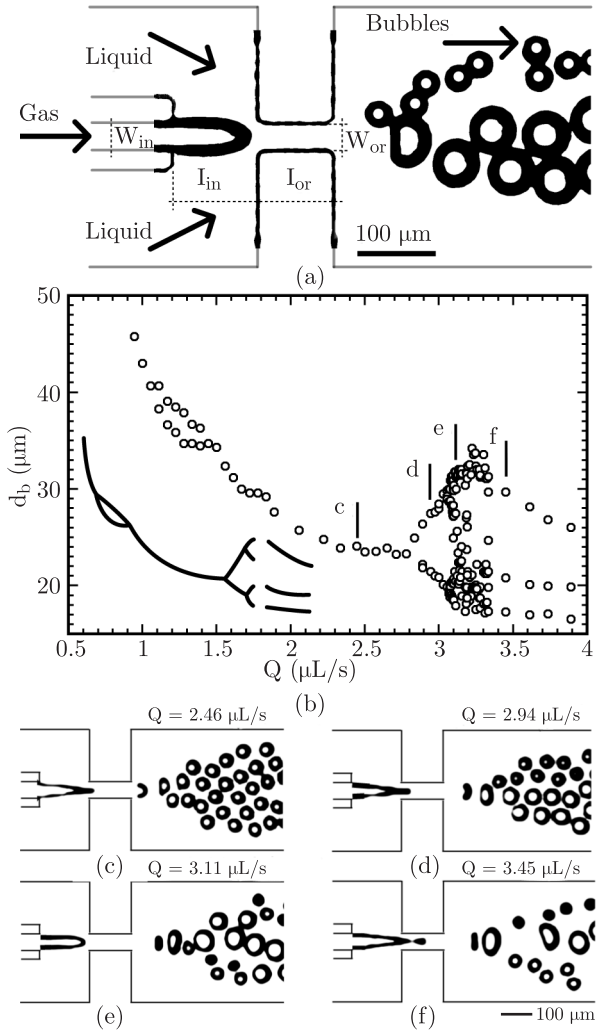

Fig. 5. An optical micrograph of the flow-focusing bubble generator comprising a planar network of channels fabricated in poly(dimethylsiloxane) and having a uniform height of 25 μm. The relevant dimensions are plotted in the figure: the width of the inlet channel ($w_{\rm in} = 30$ μm), the distance between the inlet channel and the orifice ($l_{\rm in} = 100$ μm), the width of the orifice ($w_{\rm or} = 30$ μm), and the length of the orifice ($l_{\rm or} = 100$ μm). The original micrograph is shown in black; the grey lines extend the contours of the walls (a). Bifurcation diagram showing the diameters of the bubbles as a function of the flow-rate Q of the liquid ($\mu = 0.9$ mPa s) for constant pressure ($p = 76$ kPa) of gas. The first bifurcation occurs at $Q = 1.06$ μL/s. It is followed by period-halving at $Q = 1.44$ μL/s. At $Q = 3.3$ μL/s, the first of a cascade of period-doubling bifurcations occurs. The cascade leads to chaos which, upon further increase of Q, gives way to a stable period-3 cycle. The solid line shows an outline of the bifurcation diagram (not to scale). The letters mark the rates of flow at which the micrographs of the period-1,-2,-4 and -3 bubbling are shown in insets c) to f) respectively (b). Graphs are adapted (after Ref. 70)

Here D is the width of the orifice (exit channel), and d is the apparent diameter of the bubble (the diameter of the top / bottom interface). This is a different scaling than the one we found for the flow-focusing device operating at low values of Re and Ca, where the diameter scaled as a square root of

the ratio of rates of flow (5) (this follows from the fact that when the bubbles are 'squeezed' between the top and bottom channels of the planar devices, their volume is approximately proportional to the square, and not cube, of their diameter). For $(Q_{\rm gas}/Q_{\rm liquid} < 1)$, the diameters of the bubbles varied according to (7):

$$d/D \propto (Q_{\rm gas}/Q_{\rm liquid})^{2/5}. \quad (7)$$

As we will describe it in the following sections, these scaling is characteristic for bubbling that occurs in a flow-focusing device operated at high values of Re.

Cubaoud et al. [76] used a planar system similar to the flow-focusing geometry [28,31] for formation of bubbles in aqueous solutions at a range of sizes of the bubbles and the volume fraction of the gaseous phase. Their study [76] focused on the rheological properties of suspensions of bubbles in capillaries with square cross-sections. Kawaji et al. [77] studied in detail the stability of long gaseous plugs in square capillaries.

3. Transition to high values of Reynolds numbers

3.1. Non-linear dynamics. The planar flow-focusing system (Fig. 1) generates monodisperse bubbles following the mechanism depicted in section 2 only when the capillary number is sufficiently small. An increase of the rate of flow of the liquid Q results in an increase in the frequency of formation of bubbles and above a certain critical frequency $f_{\rm CR}$, the process of break-up undergoes a period-doubling bifurcation, and, instead of a series of identical bubbles, the system produces sequences of two bubbles of different sizes. The tip of the stream of gas penetrates the orifice, breaks, and releases the first bubble, it than retracts, advances again, releases a second bubble of a different size, and the sequence repeats. Further increase of Q results in a range of non-linear phenomena: cascades of period doubling and halving bifurcations, and chaotic bubbling. We show a graph illustrating the diameters of the bubbles obtained for different values of Q in a system fed with gas at a constant pressure p. The sequence of non-linear transitions between different modes of bubbling shown in Fig. 5 includes period-doubling bifurcation, followed by a period halving one, and a cascade of period-doubling bifurcations with recognizable limit cycles of order two and four, seemingly random bubbling, and – at the highest values of Q – a stable period-3 behaviour, which persisted up to the rate of flow at which the stream of gas retracted upstream of the gas-inlet channel.

The non-linear behaviour of the flow-focusing bubble generator adds to the long history of studies on the dynamics of bubbling, originated by the work of Helsby and Tuson, who observed higher-order periodic and chaotic bubbling from a submerged nozzle [78,79] that injected bubbles into a stationary fluid. Their research was followed by a number of studies on similar systems [80–84]. By inspecting a range of viscosities and rates of flow of the liquid, and pressures applied to the stream of gas, we found that the critical frequency at which the first bifurcation of the process of bubbling occurs depends only weakly on the viscosity of the liquid. The non-linear dynamics of the flow-focusing bubble generator is most plausibly governed by the interplay between inertial and interfacial stresses. This finding suggests a similarity between the dynamics of the flow-focusing bubble generator and that of a dripping faucet – a system that is an archetypal example of non-linear behaviour in fluid mechanics [85–91].

Although we did not probe the behaviour of the system at different scales, the finding that the bifurcations root from the interplay between the inertial and interfacial effects suggests that promotion of monodisperse bubbling should be possible by reducing the size of the flow-focusing (FF) device. Smaller length scales for the evolution and relaxation of the gas-liquid interface should decrease the magnitude of the inertial stresses and result in larger values of the critical frequencies of bubbling at which the bifurcations occur [70].

4. Formation of bubbles at high values of Reynolds and Weber numbers

One of the first systems that demonstrated high-throughput formation of monodisperse bubbles with diameters in the range of tens to hundreds of micrometers, was an axi-symmetric flow-focusing device [2,3]. In this system (Fig. 6) the gas is delivered through a capillary which terminates a few hundred micrometers upstream of an orifice – a hole of a diameter D = 100 or 200 μm – fabricated in a metal plate (50 μm thick). The liquid flows around the capillary that delivers gas and into the orifice. The flow of liquid focuses the tip of the stream of gas into a cusp-like geometry with a thin ligament extending into – and through – the orifice. This ligament bulges into a growing bubble downstream of the orifice and breaks at stunningly constant frequencies. The frequency of bubbling depends on the rates of flow of the two fluids and ranges from 2×10^4 to about 10^6 Hz (the maximum of measured frequency corresponds to an experimental limitation in resolution of imaging, and not to physical limits of the phenomenon). We used a range of liquid solutions (ethanol-water and glycerol-water with the surfactant Tween 80) with densities from 950 to 1170 kgm^{-3}, viscosities from 1.2 to 31 mPas, and values of interfacial tension from 33 to 63 mNm^{-1}. Typical values of the rate of flow of liquid and gas ranged from 2.7 to 20 mL/min and from 18 to 2400 μL/min, respectively. The flow of the fluids typically proceeded at high values of Reynolds numbers: Re calculated for the liquid flowing through the orifice ranged from 50 to 1400, and the dynamics of flow is dominated by inertial effects. The diameter of the micro-jet of gas, that breaks-up into bubbles can be calculated on the basis of an assumption that viscous effects are negligible. Using this jet diameter, one finds that the interfacial stresses are in general weak in comparison with the inertial ones in the jet dynamics: the corresponding Weber numbers for the calculated jet diameter range from the value of 2 to 17. In addition, the Weber numbers calculated with the use of bubble diameters as the length-scale range from about 40 to 200. Although interfacial stresses and stability influence the length of the ligament of gas, the condition for break-up, and the mechanism which determines the volume of the bubbles

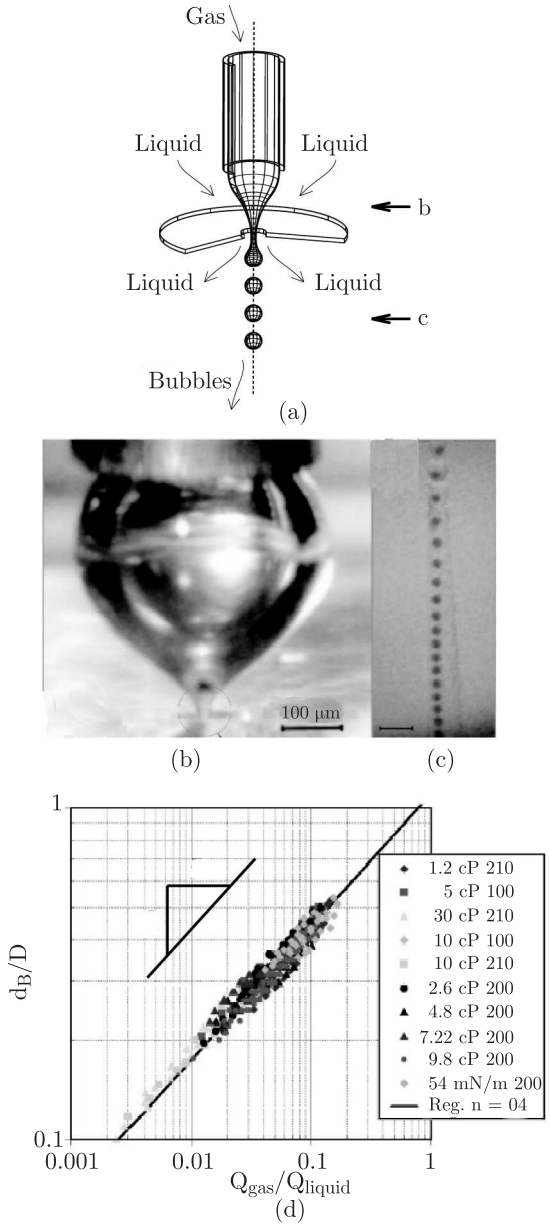

Fig. 6. A schematic illustration of the axi-symmetric flow-focusing bubble generator. The gas is delivered from a capillary that runs along the axis of the device, and is focused by the liquid flowing into a small orifice. The gaseous ligament breaks downstream of the orifice as a result of the competition of two distinct inertial stresses exerted on the growing bubble by the liquid (a). Inset b) and c) show micrographs of the focused stream of gas and bubbles produced in this device, respectively. Inset d) shows the experimental verification of the scaling of the size of the bubbles with the ratio of the rates of flow of gas and liquid. Insets b and c adapted (after Ref. 2), and inset d (after Ref. 3)

generated in the axi-symmetric FF device can be explained by the balance of two types of inertial stresses exerted i) by the growing bubble on the fluid downstream and ii) by the fluid flowing out of the orifice on the growing bubbles. A growing bubble displaces – and accelerates – the fluid downstream of it and this fluid counteracts on the bubble with a stress oriented upstream. This stress can be calculated on the basis of the rate of growth of the bubble: $v_{\mathrm{growth}} \propto Q_{\mathrm{gas}}/d_b$, where d_b is the diameter of the bubble and can be shown [3] to be on the order given by Eq. 8:

$$dv_{\mathrm{growth}}/dt \sim O(Q_{\mathrm{gas}}^2 d_b^{-5}). \tag{8}$$

. The liquid flowing out of the orifice – at an approximate rate of $v_{\mathrm{outflow}} \approx Q_{\mathrm{liquid}}/D^2$ – diverges from the axis in the radial direction and exerts a stress on the growing bubble. This stress is oriented downstream and is of a magnitude (9):

$$v_{\mathrm{outflow}} \nabla v_{\mathrm{outflow}} \sim O(Q_{\mathrm{liquid}}^2 D^{-5}). \tag{9}$$

In the beginning of the growth of the bubbles the unsteady term (7) dominates the convective term (8). As the bubble grows, the unsteady term (oriented upstream) decreases and the convective term (oriented downstream) increases. Bubbles break-off when the two terms balance, and this condition can be used to determine the final diameter of the bubbles as (10):

$$d_b/D \propto (Q_{\mathrm{gas}}/Q_{\mathrm{liquid}})^{2/5}. \tag{10}$$

We found that this scaling agrees closely with the measurements that we took for a wide range of rates of flow of the two fluids and viscosity of the liquid (Fig. 6d); in our experiments with this axisymmetric configuration, we varied the value of $(Q_{\mathrm{gas}}/Q_{\mathrm{liquid}})$ from about 0.001 to about 0.18.

5. Conclusions

We have reviewed results on the formation of bubbles in two different types of micro flow-focusing devices. The first type of system encompasses planar devices that typically operate under conditions in which the flow of the liquid is dominated by viscous effects, and the evolution of the interface is dominated by interfacial stresses. The dynamics of break-up is governed by the evolution of pressure in the streams of liquid and gas. The narrow distribution of sizes of bubbles produced in these devices is a consequence of this interplay of forces, and a quasi-static character of the evolution of the gas-liquid interface during break-up of the stream of gas. The advantages of the planar systems include i) the ease of fabrication of large numbers of them on a single chip with the use of soft-lithography, ii) the ability to tune the size of the bubbles and the volume fraction of the gaseous phase independently.

The second type of system is axi-symmetric and typically operates at high values of Reynolds and Weber numbers: that is, with inertial effects dominating both the flow of the liquid and the dynamics of the interface. In this system, the monodisperse character of the bubbles is achieved via a balance of two inertial stresses acting on the growing bubble: one preventing, and one promoting, break-off. For given – constant – rates of flow of the two fluids fed into the device, the system locks into periodic dynamics and produces monodisperse bubbles. This device is suitable for formation of bubbles at high rates s; in our experiments from 20 thousands to more than 500 thousands per second.

The systems presented in this review are capable of producing bubbles at high rates (up to 10^4–10^6 bubbles per second from a single device) with a precise control over their size

(from few micrometers to a fraction of a millimetre in the diameter) and volume fraction (from 0 to 1). These features make these and other microfluidic devices attractive for generation of suspensions of bubbles for a range of applications – from preparation of ultra-sound contrast agents [92,93], or for use in ultrasonic techniques for treating tumours [94], to synthesis of meso-porous materials [95]. Bubbles find growing number of uses in the chemical processing in micro-chip laboratories, from the use of slug flow for mixing, homogenization of residence times and segmentation [57,63–66], through acoustic techniques for mixing [96] and pumping [97] to engineering the flow of foams in microchannels for transport of samples [98,99]. Increasing our understanding of interfacial dynamics in micro-devices, and of the design of optimized systems, should help broaden the range of these applications.

Acknowledgements. We thank our colleague Prof. Howard Stone (Harvard University) for discussions, and for his continuing help in understanding multiphase flows in microfluidic systems. P.G. acknowledges financial support from the Foundation for Polish Science. The work at Harvard University was supported by the U.S. Department of Energy (DE-FG02-00ER45852). We thank the Harvard MRSEC for the use of high-speed cameras and clean-room facilities. AMGC wishes to thank Dr. J.M. Gordillo, M. Hoc, V. Marandat, N. Ouarty, T. Prevost, J.L. Sampedro and S. Vidal for their help in the experiments, and to the Spanish Ministry of Education and Science, grant no. DPI2002-04305-C02-02.

REFERENCES

[1] T. Thorsen, R.W. Roberts, F.H. Arnold, and S.R. Quake, "Dynamic pattern formation in a vesicle-generating microfluidic device", *Phys. Rev. Lett.* 86, 4163 (2001).

[2] A.M. Ganan-Calvo and J.M. Gordillo, "Perfectly monodisperse microbubbling by capillary flow focusing." *Phys. Rev. Lett.* 87, 274501 (2001).

[3] A.M. Ganan-Calvo, "Perfectly monodisperse microbubbling by capillary flow focusing: An alternate physical description and universal scaling", *Phys. Rev. E* 69, 027301 (2004).

[4] J. Eggers, "Nonlinear dynamics and breakup of free-surface flows", *Rev. Mod. Phys.* 69, 865 (1997).

[5] P.J.A. Kenis, R.F. Ismagilov, and G.M. Whitesides, "Microfabrication inside capillaries using multiphase laminar flow patterning", *Science* 285, 83 (1999).

[6] D.C. Duffy, J.C. McDonald, O.J.A. Schueller, and G.M. Whitesides, "Rapid prototyping of microfluidic systems in poly(dimethylsiloxane)", *Anal. Chem.* 70, 4974 (1998).

[7] J.C. McDonald, D.C. Duffy, J.R. Anderson, D.T. Chiu, H. Wu, O.J.A. Schueller, and G.M. Whitesides, "Fabrication of microfluidic systems in poly(dimethylosiloxane)", *Electrophoresis* 21, 27 (2000).

[8] J.W. Hong and S.R. Quake, "Integrated nanoliter systems", *Nat. Biotech.* 21, 1179 (2003).

[9] S.K.W. Dertinger, X.Y. Jiang, Z.Y. Li, V.N. Murthy, and G.M. Whitesides, "Gradients of substrate-bound laminin orient axonal specification of neurons", *Proc. Natl. Acad. Sci. U. S. A.* 99, 12542 (2002).

[10] E.M. Luchetta, J.H. Lee, L.A. Fu, N.H. Patel, and R.F. Ismagilov, "Dynamics of Drosphila embryonic patterning network perturbed in space and time using microfluidics", *Nature* 434, 1134 (2005).

[11] T.A. Thorsen, "Microfluidic tools for high-throughput screening", *BioTechniques* 36, 197 (2004).

[12] S.K. Sia, V. Linder, B.A. Parviz, A. Siegel, and G.M. Whitesides, "An integraded approach to a portable and low-cost immunoassay for resource-poor settings", *Angew. Chem., Int. Ed. Engl.* 43, 498 (2004).

[13] P. Angenendt, J. Glokler, Z. Konthur, H. Lehrach, and D.J. Cahill, "3D protein microarrays: Performing multiplex immunoassays on a single chip", *Anal. Chem.* 75, 4368 (2003).

[14] Z.T. Cygan, J.T. Cabral, K.L. Beers, and E.J. Amis, "Microfluidic platform for the generation of organic-phase microreactors", *Langmuir* 21, 3629 (2005).

[15] O.A. Basaran, "Small-scale free surface flows with breakup: Drop formation and emerging applications", *AIChE J.* 48, 1842 (2002).

[16] H. A. Stone, A.D. Stroock, and A. Ajdari, "Engineering flows in small devices: Microfluidics toward a lab-on-a-chip", *Annu. Rev. Fluid Mech.* 36, 381 (2004).

[17] P. Garstecki, M.J. Fuerstman, H.A. Stone, and G.M. Whitesides, "Formation of droplets and bubbles in microfluidic T-junction geometries: scaling and mechanism of break-up", *Lab Chip*, (to be published).

[18] J.D. Tice, A.D. Lyon, and R.F. Ismagilov, "Effects of viscosity on droplet formation and mixing in microfluidic channels", *Anal. Chim. Acta* 507, 73 (2004).

[19] B. Blackmore, D.Q. Li, and J. Gao, "Detachment of bubbles in slit microchannels by shearing flow", *J. Colloid Interface Sci.* 241, 514 (2001).

[20] H. Song and R.F. Ismagilov, "Millisecond kinetics on a microfluidic chip using nanoliters of reagents", *J. Am. Chem. Soc.* 125, 14613 (2003).

[21] C.J. Gerdts, D.E. Sharoyan, and R.F. Ismagilov, "A synthetic reaction network: Chemical amplification using nonequilibrium autocatalytic reactions coupled in time", *J. Am. Chem. Soc.* 126, 6327 (2004).

[22] B. Zheng, L.S. Roach, and R.F. Ismagilov, "Screening of protein crystallization conditions on a microfluidic chip using nanoliter-size droplets", *J. Am. Chem. Soc.* 125, 11170 (2003).

[23] B. Zheng, J.D. Tice, L.S. Roach, and R.F. Ismagilov, "Nanoliter droplet-based microfluidic system for evaluating protein crystallization conditions with on-chip diffraction", *Abstr. Pap. Am. Chem. Soc.* 228, U533 (2004).

[24] D. Dendukuri, K. Tsoi, T.A. Hatton, and P.S. Doyle, "Controlled synthesis of nonspherical microparticles using microfluidics", *Langmuir* 21, 2113 (2005).

[25] S. Okushima, T. Nisisako, T. Torii, and T. Higuchi, "Controlled production of monodisperse double emulsions by two-step droplet breakup in microfluidic devices", *Langmuir* 20, 9905 (2004).

[26] A.S. Utada, E. Lorenceau, D.R. Link, P.D. Kaplan, H.A. Stone, and D.A. Weitz, "Monodisperse double emulsions generated from a microcapillary device", *Science* 308, 537 (2005).

[27] S. Takeuchi, P. Garstecki, D.B. Weibel, and G.M. Whitesides, "An axisymmetric flow-focusing microfluidic device", *Adv. Mater. (Weinheim, Fed. Repub. Ger.)* 17, 1067 (2005).

[28] S.L. Anna, N. Bontoux, and H.A. Stone, "Formation of dispersions using "flow focusing" in microchannels", *Appl. Phys. Lett.* 82, 364 (2003).

[29] Q.Y. Xu and M. Nakajima, "The generation of highly monodisperse droplets through the breakup of hydrodynamically fo-

cused microthread in a microfluidic device", *Appl. Phys. Lett.* 85, 3726 (2004).

[30] T. Ward, M. Faivre, M. Abkarian, and H.A. Stone, *Microfluidic Flow Focusing: Drop Size and Scaling in Pressure versus Flow-Rate-Driven Fluid Pumping*, (to be published).

[31] P. Garstecki, I. Gitlin, W. Diluzio, E. Kumacheva, H.A. Stone, and G.M. Whitesides, "Formation of monodisperse bubbles in a microfluidic flow-focusing device", *Appl. Phys. Lett.* 85, 2649 (2004).

[32] P. Garstecki, H.A. Stone, and G.M. Whitesides, "Mechanism for flow-rate controlled breakup in confined geometries: A route to monodisperse emulsions", *Phys. Rev. Lett.* 94, 164501 (2005).

[33] J.M. Gordillo, Z.D. Cheng, A.M. Ganan-Calvo, M.Marquez, and D.A. Weitz, "A new device for the generation of microbubbles", *Phys. Fluids* 16, 2828 (2004).

[34] D.R. Link, S.L. Anna, D.A. Weitz, and H.A. Stone, "Geometrically mediated breakup of drops in microfluidic devices", *Phys. Rev. Lett.* 92, 054503 (2004).

[35] S. Sugiura, M. Nakajima, S. Iwamoto, and M. Seki, "Interfacial tension driven monodispersed droplet formation from microfabricated channel array", *Langmuir* 17, 5562 (2001).

[36] I. Kobayashi, X.F. Lou, S. Mukataka, and M. Nakajima, "Preparation of monodisperse water-in-oil-in-water emulsions using microfluidization and straight-through microchannel emulsification", *J. Am. Oil Chem. Soc.* 82, 65 (2005).

[37] H.J. Liu, M. Nakajima, and T. Kimura, "Production of monodispersed water-in-oil emulsions using polymer microchannels", *Journal of the American Oil Chemists Society* 81, 705 (2004).

[38] C. P. Steinert, I. Goutier, O. Gutmann, H. Sandmaier, M. Daub, B. de Heij, and R. Zengerle, "A highly parallel picoliter dispenser with an integrated, novel capillary channel structure", *Sens. Actuators A* 116, 171 (2004).

[39] S.Q. Xu, Z.H. Nie, M. Seo, P. Lewis, E. Kumacheva, H.A. Stone, P. Garstecki, D.B. Weibel, I. Gitlin, and G.M. Whitesides, "Generation of monodisperse particles by using microfluidics: Control over size, shape, and composition", *Angew. Chem., Int. Ed. Engl.* 44, 724 (2005).

[40] W.J. Jeong, J.Y. Kim, J. Choo, E.K. Lee, C.S. Han, D.J. Beebe, G.H. Seong, and S.H. Lee, "Continuous fabrication of biocatalyst immobilized microparticles using photopolymerization and immiscible liquids in microfluidic systems", *Langmuir* 21, 3738 (2005).

[41] T. Nisisako, T. Torii, and T. Higuchi, "Novel microreactors for functional polymer beads", *Chem. Eng. J.* 101, 23 (2004).

[42] W.J. Jeong, J.Y. Kim, S. Kim, S.H. Lee, G. Mensing, and D.J. Beebe, "Hydrodynamic microfabrication via "on the fly" photopolymerization of microscale fibers and tubes", *Lab Chip* 4, 576 (2004).

[43] Z.H. Nie, S.Q. Xu, M. Seo, P.C. Lewis, and E. Kumacheva, "Polymer particles with various shapes and morphologies produced in continuous microfluidic reactors", *J. Am. Chem. Soc.* 127, 8058 (2005).

[44] L. Martin-Banderas, M. Flores-Mosquera, P. Riesco-Chueca, A. Rodriguez-Gil, A. Cebolla, S. Chavez, and A.M. Ganan-Calvo, "Flow focusing: A versatile technology to produce size-controlled and specific-morphology microparticles", *Small* 1, 688 (2005).

[45] S. Sugiura, T. Oda, Y. Izumida, Y. Aoyagi, M. Satake, A. Ochiai, N. Ohkohchi, and M. Nakajima, "Size control of calcium alginate beads containing living cells using micro-nozzle array", *Biomaterials* 26, 3327 (2005).

[46] M. Seo, Z.H. Nie, S.Q. Xu, P.C. Lewis, and E. Kumacheva, "Microfluidics: From dynamic lattices to periodic arrays of polymer disks", *Langmuir* 21, 4773 (2005).

[47] D. Rudhardt, A. Fernandez-Nieves, D.R. Link, and D.A. Weitz, "Phase switching of ordered arrays of liquid crystal emulsions", *Appl. Phys. Lett.* 82, 2610 (2003).

[48] D. Belder, "Microfluidics with droplets", *Angew. Chem., Int. Ed. Engl.* 2005, 23 (2005).

[49] K. Hosokawa, T. Fujii, and I. Endo, "Handling of picoliter liquid samples in a poly(dimethylsiloxane)-based microfluidic device", *Anal. Chem.* 71, 4781 (1999).

[50] B. Zheng and R.F. Ismagilov, "A microfluidic approach for screening submicroliter volumes against multiple reagents by using preformed arrays of nanoliter plugs in a three-phase liquid/liquid/gas flow", *Angew. Chem., Int. Ed. Engl.* 44, 2520 (2005).

[51] Y.C. Tan, J.S. Fisher, A.I. Lee, V. Cristini, and A.P. Lee, "Design of microfluidic channel geometries for the control of droplet volume, chemical concentration, and sorting", *Lab Chip* 4, 292 (2004).

[52] H. Song, M.R. Bringer, J.D. Tice, C.J. Gerdts, and R.F. Ismagilov, "Experimental test of scaling of mixing by chaotic advection in droplets moving through microfluidic channels", *Appl. Phys. Lett.* 83, 4664 (2003).

[53] M.Y. He, J.S. Edgar, G.D.M. Jeffries, R.M. Lorenz, J.P. Shelby, and D.T. Chiu, "Selective encapsulation of single cells and subcellular organelles into picoliter- and femtoliter-volume droplets", *Anal. Chem.* 77, 1539 (2005).

[54] Y. Fouillet and J.L. Achard, "Digital microfluidic and biotechnology", *C.R. l'Academie. Sci., Ser. II Univers* 5, 577 (2004).

[55] H. Ren, R.B. Fair, and M.G. Pollack, "Automated on-chip droplet dispensing with volume control by electro-wetting actuation and capacitance metering", *Sensors and Actuators B-Chemical* 98, 319 (2004).

[56] S.K. Cho, H.J. Moon, and C.J. Kim, "Creating, transporting, cutting, and merging liquid droplets by electrowetting-based actuation for digital microfluidic circuits", *J. MEMS* 12, 70 (2003).

[57] V. Srinivasan, V.K. Pamula, and R.B. Fair, "An integrated digital microfluidic lab-on-a-chip for clinical diagnostics on human physiological fluids", *Lab Chip* 4, 310 (2004).

[58] D.E. Kataoka and S.M. Troian, "Patterning liquid flow on the microscopic scale", *Nature* 402, 794 (1999).

[59] L.R. Snyder and H.J. Adler, "Dispersion in segmented flow through glass tubing in continuous-flow analysis – nonideal model", *Anal. Chem.* 48, 1022 (1976).

[60] L.R. Snyder and H.J. Adler, "Dispersion in segmented flow through glass tubing in continuous-flow analysis – ideal model", *Anal. Chem.* 48, 1017 (1976).

[61] S.E. Burns, S. Yiacoumi, and C. Tsouris, "Microbubble generation for environmental and industrial separations", *Sep. Purif. Tech.* 11, 221 (1997).

[62] A. Berthod, M.A. Rodriguez, M. Girod, and D.W. Armstrong, "Use of microbubbles in capillary electrophoresis for sample segregation when focusing microbial samples", *J. Sep. Sci.* 25, 988 (2002).

[63] A. Grodrian, J. Metze, T. Henkel, K. Martin, M. Roth, and J.M. Kohler, "Segmented flow generation by chip reactors for highly parallelized cell cultivation", *Biosens. Bioelectr.* 19, 1421 (2004).

[64] A. Gunther, S.A. Khan, M. Thalmann, F. Trachsel, and K.F. Jensen, "Transport and reaction in microscale segmented gas-liquid flow", *Lab Chip* 4, 278 (2004).

[65] A. Gunther, M. Jhunjhunwala, M. Thalmann, M.A. Schmidt, and K.F. Jensen, "Micromixing of miscible liquids in segmented gas-liquid flow", *Langmuir* 21, 1547 (2005).
[66] P. Garstecki, M.A. Fischbach, and G.M. Whitesides, "Design for mixing using bubbles in branched microfluidic channels", *Appl. Phys. Lett.* 86, 244108 (2005).
[67] J.R. Burns and C. Ramshaw, "The intensification of rapid reactions in multiphase systems using slug flow in capillaries", *Lab Chip* 1, 10 (2001).
[68] G.I. Taylor, "Deposition of a viscous fluid on the wall of a tube", *J. Fluid Mech.* 10, 161 (1961).
[69] S.A. Khan, A. Gunther, M.A. Schmidt, and K.F. Jensen, "Microfluidic synthesis of colloidal silica", *Langmuir* 20, 8604 (2004).
[70] P. Garstecki, M.J. Fuerstman, and G.M. Whitesides, "Nonlinear dynamics of a flow-focusing bubble generator: An inverted dripping faucet", *Phys. Rev. Lett.* 94, 234502 (2005).
[71] R. Dreyfus, P. Tabeling, and H. Willaime, "Ordered and disordered patterns in two-phase flows in microchannels", *Phys. Rev. Lett.* 90, 144505 (2003).
[72] K. Brakke, `http://www.susqu.edu/facstff/b/brakke/evolver`
[73] H.A. Stone, "On lubrication flows in geometries with zero local curvature", *Chem. Eng. Sci.* 60, 4838 (2005).
[74] I. Cohen and S.R. Nagel, "Scaling at the selective withdrawal transition through a tube suspended above the fluid surface", *Phys. Rev. Lett.* 88, 074501 (2002).
[75] I. Cohen, H. Li, J.L. Hougland, M. Mrksich, and S.R. Nagel, "Using selective withdrawal to coat microparticles." *Science* 292, 265 (2001).
[76] T. Cubaud and C.M. Ho, "Transport of bubbles in square microchannels", *Phys. Fluids* 16, 4575 (2004).
[77] M. Kawaji and P.M.Y. Chung, "Adiabatic gas-liquid flow in microchannels", *Microscale Thermophys. Eng.* 8, 239 (2004).
[78] K.R. Tuson, "Single exposure photography of a high speed event", *Brit. J. Appl. Phys.* 6, 99 (1955).
[79] F.W. Helsby and K.R. Tuson, *Research* 8, 270 (1955).
[80] D.J. Tritton and C. Egdell, "Chaotic bubbling", *Phys. Fluids* 5, 503 (1993).
[81] A. Tufaile and J.C. Sartorelli, "Henon-like attractor in air bubble formation", *Phys. Lett. A* 275, 211 (2000).
[82] A. Tufaile and J.C. Sartorelli, "Chaotic behavior in bubble formation dynamics", *Physica A* 275, 336 (2000).
[83] L.J. Mittoni, M.P. Schwarz, and R.D. Lanauze, "Deterministic chaos in the gas inlet pressure of gas-liquid bubbling system", *Phys. Fluids* 7, 891 (1995).
[84] M.Y. Liu, Z.D. Hu, and J.H. Li, "Multi-scale characteristics of chaos behavior in gas-liquid bubble columns", *Chem. Eng. Commun.* 191, 1003 (2004).
[85] K. Kiyono, T. Katsuyama, T. Masunaga, and N. Fuchikami, "Picture of the low-dimensional structure in chaotic dripping faucets", *Phys. Lett. A* 320, 47 (2003).
[86] B. Ambravaneswaran, S.D. Phillips, and O.A. Basaran, "Theoretical analysis of a dripping faucet", *Phys. Rev. Lett.* 85, 5332 (2000).
[87] B. Ambravaneswaran, H.J. Subramani, S.D. Phillips, and O.A. Basaran, "Dripping-jetting transitions in a dripping faucet", *Phys. Rev. Lett.* 93, 034501 (2004).
[88] P. Coullet, L. Mahadevan, and C. Riera, "Return map for the chaotic dripping faucet", *Prog. Theor. Phys. Suppl.*, 507 (2000).
[89] P. Coullet, L. Mahadevan, and C. Riera, "Hydrodynamical models for the chaotic dripping faucet", *J. Fluid Mech.* 526, 1 (2005).
[90] A. dInnocenzo and L. Renna, "Analytical solution of the dripping faucet dynamics", *Phys. Lett. A* 220, 75 (1996).
[91] P.M.C. Deoliveira and T.J.P. Penna, "Simulating the Complex Behavior of a Leaky Faucet", *J. Stat. Phys.* 73, 789 (1993).
[92] P.J.A. Frinking, A. Bouakaz, J. Kirkhorn, F.J. Ten Cate, and N. de Jong, "Ultrasound contrast imaging: Current and new potential methods", *Ultrasound in Medicine and Biology* 26, 965 (2000).
[93] E. Stride and N. Saffari, "Microbubble ultrasound contrast agents: a review", *Proc. Inst. Mech. Eng., IMechE Conf.* 217, 429 (2003).
[94] M.R. Bailey, V.A. Khokhlova, O.A. Sapozhnikov, S.G. Kargl, and L.A. Crum, "Physical mechanisms of the therapeutic effect of ultrasound – (A review)", *Acoust. Phys.* 49, 369 (2003).
[95] A. M. Kraynik, "Foam structure: From soap froth to solid foams", *Mater. Res. Soc. Bull.* 28, 275 (2003).
[96] R.H. Liu, R. Lenigk, and P. Grodzinski, "Acoustic micromixer for enhancement of DNA biochip systems", *J. Microlith. Microfab. Microsystems* 2, 178 (2003).
[97] P. Marmottant and S. Hilgenfeldt, "Controlled vesicle deformation and lysis by single oscillating bubbles", *Nature* 423, 153 (2003).
[98] S. Hutzler, D. Weaire, F. Elias, and E. Janiaud, "Juggling with bubbles in cylindrical ferrofluid foams", *Philos. Mag. Lett.* 82, 297 (2002).
[99] W. Drenckhan, S.J. Cox, G. Delaney, H. Holste, D. Weaire, and N. Kern, "Rheology of ordered foams – on the way to discrete microfluidics", *Colloids Surf.* A 263, 52 (2005).